Strong correlation between ferromagnetism and oxygen deficiency in Cr-doped $In_2O_{3-\delta}$ nanostructures

G. Z. Xing,[1] J. B. Yi,[2] D. D. Wang,[1] L. Liao,[1] T. Yu,[1] Z. X. Shen,[1] C. H. A. Huan,[1] T. C. Sum,[1] J. Ding,[2] and T. Wu[1,*]

[1]*Division of Physics and Applied Physics, School of Physical and Mathematical Sciences, Nanyang Technological University, Singapore 637371, Singapore*

[2]*Department of Materials Science and Engineering, National University of Singapore, Singapore 119260, Singapore*

(Received 22 November 2008; published 5 May 2009)

Single-crystalline Cr-doped $In_2O_{3-\delta}$ nanostructures with diverse morphologies including nanotowers, nanowires, and octahedrons are synthesized by using a vapor transport method. X-ray photoelectron spectroscopy results indicate that the as-grown samples contain 3 at. % Cr and are significantly oxygen deficient. The large surface-to-volume ratio in the nanostructures enhances their susceptibility to the postsynthesis treatments; high-temperature annealing in air boosts the oxygen contents in the samples, which is accompanied by a weakened defect-related emission in the photoluminescence spectra. Magnetization measurements on the as-grown and the annealed nanostructures suggest room-temperature ferromagnetism, and importantly the ferromagnetism is stronger in samples with higher oxygen deficiency. Electronic band alterations as a result of the Cr doping and the oxygen vacancies as well as the formation of bound magnetic polarons are suggested to play important roles in stabilizing the long-range ferromagnetism.

DOI: 10.1103/PhysRevB.79.174406 PACS number(s): 75.50.Pp, 81.07.−b, 75.75.+a

I. INTRODUCTION

The prospect of incorporating magnetic properties into semiconductors has provoked intensive research on developing diluted magnetic semiconductors (DMSs).[1–3] Since the theoretical prediction of room-temperature ferromagnetism (RTFM) in Mn-doped *p*-type ZnO and GaN,[4] considerable efforts have been concentrated on exploring new DMS to enable potential applications in spintronics. Both experimental and theoretical works on DMS with RTFM have been reported, in particular, for a few 3*d* transition-metal-doped wide-gap semiconductors, such as TiO_2, ZnO, and SnO_2.[5–10] Among the oxide hosts, In_2O_3 (IO) is a transparent semiconductor with a body-centered-cubic bixbyite structure (space group $Ia\bar{3}$, lattice constant $a=10.114$ Å, and JCPDF # 71–2195) and a direct band gap of 3.75 eV. Its conducting alloy with Sn, i.e., ITO has been widely used in electronics, photovoltaic devices, liquid crystal displays, and light emitting diodes.[11,12] Recently, IO-based DMSs have attracted lots of attention and RTFM was reported in IO doped or codoped with Ti, V, Cr, Mn, Fe, and Ni.[13–17]

Among these elements, Cr doping is particularly interesting and has attracted lots of attention.[18–22] A Curie temperature of 850 K was reported on Cr-doped IO (Cr:IO) thin films.[18] Unlike many other metals, Cr itself is antiferromagnetic and it would not induce an extrinsic ferromagnetism even if Cr clustering occurs. Furthermore, trivalent Cr^{3+} ions exhibit $3d^3$ high-spin configuration, which may help to generate large magnetic moments in the host semiconductors. Most of the previous studies on doped IO were focused on bulks and thin films. Only recently RTFM was reported for Fe-doped IO nanocrystals.[23] So far there have been few reports on one-dimensional IO-based DMS nanomaterials. Compared with the bulk counterparts, nanostructures are characterized by larger surface-to-volume ratios and are more amenable to postgrowth treatments, such as thermal annealing[19] and chemical modifications,[24] which bring out additional freedoms to tailor the magnetic properties in DMS nanostructures.

In this work, we carried out a systematic investigation on the magnetic properties of Cr:IO nanostructures. By tuning the growth conditions in the vapor transport synthesis, we obtained nanostructures with different morphologies including nanotowers, nanowires, and octahedrons. Regardless of the morphologies, RTFM was observed in the as-grown oxygen-deficient samples and the ferromagnetism was significantly weakened after annealing in air, which suggests a strong correlation between the ferromagnetism and the oxygen deficiency. The origin of the observed magnetism was discussed in terms of the defect-assisted formation of bound magnetic polarons and the doping-induced alteration of the host band structure. Our studies suggest that a precise control on the doping characteristics and the defect structures must be achieved before DMS nanostructures can be used as building blocks in nanoscale spintronic devices.

II. EXPERIMENT DETAILS

We successfully synthesized three types of Cr:IO nanostructures, i.e., nanotowers, nanowires, and octahedrons by using a chemical vapor transport method in a horizontal tube furnace. The detailed experimental setup was described in previous publications.[25,26] In a typical process, for the growth of Cr:IO nanotowers and nanowires, In_2O_3 (99.999%, Aldrich), $CrCl_2$ (99.99%, Aldrich), and graphite (99.99%, Aldrich) powders with a weight ratio of 5:0.6:4 and a total weight of 0.1 g were mixed, ground for 20 min, and then used as the source. The mixture was loaded in a slender quartz tube and inserted into a horizontal tube furnace (Lindberg/Blue Mini-Mite). Carefully cleaned silicon substrates with a dimension of ~6 mm×8 mm were sputtered with 2 nm Au films as catalyst and placed downstream from the powder mixture. Before heating to the desired temperature, the tube furnace was evacuated to $\sim 10^{-2}$ torr

(1 torr=133.32 Pa) to remove the residual oxygen. During the synthesis, high-purity argon mixed with 0.5% oxygen with a constant flow rate of 80 SCCM (standard cubic centimeter per minute) was used as the carrying gas and the products were grown under an inner pressure of ~100 torr. The temperature of the furnace was ramped to 980 or 800 °C, which led to the growth of nanotowers or nanowires. Total growth time was kept for 1 h and then the furnace was cooled down to room temperature (RT) naturally. After the reaction, a layer of light-yellow product was found on the silicon substrates. For the synthesis of Cr:IO octahedrons, the source material was a mixture of In (99.999%, Aldrich) and $CrCl_2$ powders and the growing temperature was 980 °C. The final product has a yellow color. For the synthesis of undoped IO samples, all the experimental conditions remained the same except that $CrCl_2$ was not used in the source powder.

A JEOL JSM-6700F FESEM (field emission at 5 or 10 kV) was used to investigate the morphology of samples. The crystalline structures were characterized by x-ray diffraction (XRD) using Cu Kα radiation (λ=0.15418 nm) in 2θ range from 20° to 70° with 0.005° step size. High-resolution transmission electron microscope (HRTEM) (JEOL2100F) was operated at an accelerating voltage of 300 kV. The chemical bonding states and the compositions of the products were determined by x-ray photoelectron spectroscopy (XPS) (VG ESCALAB 220i-XL system equipped with a monochromatic x-ray source) in an ultrahigh-vacuum chamber at a pressure lower than 1.0×10^{-9} torr. Peak positions are referenced to the adventitious C1*s* peak which was taken to be 285.0 eV. The relative chemical compositions were calculated by using the atomic sensitivity factors (In 3*d*5: 6; O 1*s*: 0.66; and Cr 2*p*: 2.3) after calibration and fitting to the integrated intensities of the core-level XPS peaks. The data analysis was done using XPSPEAK 4.1 software (UK Surface Analysis). Photoluminescence (PL) measurements were carried out to investigate the optical properties of the nanotowers. The samples were excited by using a He-Cd laser with 325 nm wavelength and 2 mW power. The samples were mounted on an *xyz* table which moves the samples to the intersection point of the laser beam and the optical axis to achieve better S/N ratio. The signals were collected with Olympus camera lens at RT. Raman spectra were carried out with a WITEC CRM200 Raman system. The excitation source is 532 nm (2.33 eV) laser and the samples were placed on an *x*-*y* piezo stage. The stage movement and data acquisition were controlled by using SCANCTRL SPECTROSCOPY PLUS software (WITec GmbH, Germany). Magnetization measurements were carried out on a superconducting quantum interference device (SQUID) magnetometer (Quantum Design, MPMSXL-5). Multiple curves were recorded to ensure the data reproducibility. Throughout all the experimental steps taken during synthesis and measurements, only plastic tweezers were used to avoid any unintentional contact with metals.

III. PHYSICAL PROPERTIES OF Cr:IO NANOSTRUCTURES

Since the procedures of structural and compositional characterizations are similar to all the samples, in this section we focus on the experimental results obtained on nanotowers. The oxygen content in the nanotower samples was adjusted by annealing the as-grown products at 600 °C in air for 1 h. As listed in Table I, we named the as-grown and the annealed Cr:IO nanotower samples as CIO-T-1 and CIO-T-2, respectively.

TABLE I. Morphologies and compositions of the as-grown and the annealed Cr:IO and IO nanostructures.

Sample	Morphology	Composition[a]	Annealed
CIO-T-1	Nanotowers	$(In_{0.97}Cr_{0.03})_2O_{2.57}$	No
CIO-T-2	Nanotowers	$(In_{0.97}Cr_{0.03})_2O_{2.88}$	Yes
IO-T-1	Nanotowers	$In_2O_{2.57}$	No
CIO-W-1	Nanowires	$(In_{0.97}Cr_{0.03})_2O_{2.28}$	No
CIO-W-2	Nanowires	$(In_{0.97}Cr_{0.03})_2O_{2.55}$	Yes
IO-W-1	Nanowires	$In_2O_{2.29}$	No
CIO-O-1	Octahedrons	$(In_{0.97}Cr_{0.03})_2O_{2.40}$	No
CIO-O-2	Octahedrons	$(In_{0.97}Cr_{0.03})_2O_{2.80}$	Yes
IO-O-1	Octahedrons	$In_2O_{2.42}$	No

[a]The compositions were determined by fitting to the XPS spectra.

As shown in Fig. 1(a), the towerlike tapered nanostructures were grown on the silicon substrates and their fourfold symmetry is consistent with the bixbyite structure of IO. A magnified FESEM image in Fig. 1(b) shows a faceted morphology on the side surfaces. The diameter of the nanotowers typically decreases from 200 to 30 nm along the growth direction and their lengths are several micrometers. We synthesized 24 undoped and Cr-doped IO nanotower samples; their growth and physical properties are highly reproducible. Compared with the undoped IO samples, Cr doping does not change the sample morphology. Since much less nanostructures were produced without the Au catalyst, the growth

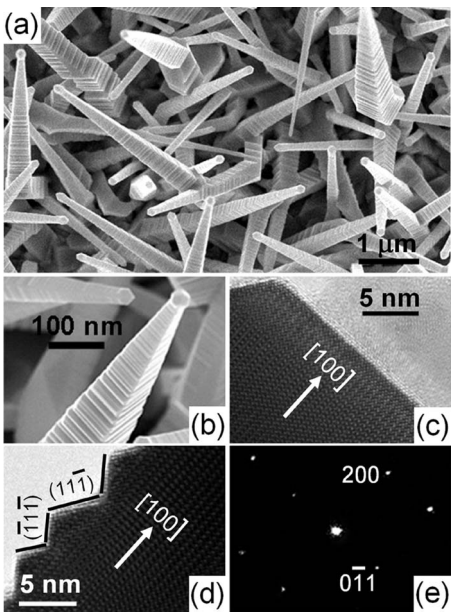

FIG. 1. (a) Low- and (b) high-magnification FESEM images of the Cr:IO nanotowers. HRTEM images taken at (c) the tip and (d) the side of a nanotower. (e) Corresponding SAED patterns.

mechanism appears to be the vapor-liquid-solid (VLS) growth.[27]

The structural characteristics of the Cr:IO nanotower samples were investigated in detail by using a HRTEM. The smooth top surface as shown in Fig. 1(c) possibly suggests a significant Au migration during the VLS growth, similar to the previous observations in other nanowire systems.[28,29] The nanotowers grow along the [100] direction, in accordance with the previous reports on undoped IO nanotowers.[30] Figure 1(d) shows that the side surfaces reconstruct into $(\bar{1}1\bar{1})$ and $(11\bar{1})$ facets, as a result of the slower growth rate along ⟨111⟩ compared with those along the ⟨100⟩ and ⟨110⟩ directions. As shown in Fig. 1(e), the selected area electron diffraction (SAED) pattern taken along the $[0\bar{1}\bar{1}]$ zone axis indicates a cubic structure with no detectable secondary phase.

Consistent with the TEM data, the XRD pattern of CIO-T-1 in Fig. 2(a) suggests the cubic bixbyite structure without any detectable impurity phase. As shown in the inset, compared with the undoped IO nanotowers sample (IO-T-1), the (222) peak of CIO-T-1 exhibits a shift of 0.06° to a larger angle, which corresponds to a decrease in the lattice constant by 0.14%. The shrinkage of lattice constant after doping can be attributed to the substitution of the smaller Cr^{3+} ions (0.76 Å) onto the In^{3+} (0.94 Å) lattice sites,[31] which indicates that Cr ions are incorporated into the IO matrix. In CIO-T-2, the annealing treatment did not introduce any new phase. The (222) peak in the annealed sample CIO-T-2 is slightly narrower compared with that of the as-grown sample CIO-T-1, which indicates an improved crystal structure after annealing.

To investigate the chemical compositions and the bonding states, XPS measurements were performed on the nanotower samples. Ar ion sputtering was carried out first for a few minutes to eliminate any potential surface contamination. The XPS results for the samples CIO-T-1 and CIO-T-2 are shown in Fig. 2(b). The survey scans show no magnetic impurity within the detection limit. Cr $2p_{3/2}$ peaks were detected at 577.5 and 577.2 eV for CIO-T-1 and CIO-T-2, respectively. The detailed scans of these peaks are shown in the insets of Fig. 2(b). The peak positions are different from Cr metal (574.0 eV), Cr^{2+} (576.0 eV), Cr^{4+} (576.3 eV), and Cr^{6+} ions (579.0 eV) but match Cr^{3+} ions (577.2 eV).[32,33] Since the extensive HRTEM, SAED, and XRD experiments did not detect substantial Cr interstitials or undesired phases containing Cr^{3+}, the XPS results suggest that Cr ions may replace the In^{3+} ions in the IO matrix. From the XPS spectra, the eventual nonstoichiometric formula for CIO-T-1 and CIO-T-2 were determined to be $(In_{0.97}Cr_{0.03})_2O_{2.57}$ and $(In_{0.97}Cr_{0.03})_2O_{2.88}$, respectively. Since the penetration depth of Al Kα XPS is several nm, after the top layers of the samples were sputtered off, the compositions determined for the nanostructures should be quite close to the actual values, which allowed quantitative comparisons among the samples. We found that the doping method consistently led to a 3 at. % Cr concentration, which is comparable to the 2 at. % chosen by Philip *et al.*[18] in their thin-film study. It is important to note that substantial oxygen vacancies exist in the as-grown Cr:IO nanotower samples. This high level of oxygen deficiency can be attributed to the incomplete oxidation during the vapor transport growth. Air annealing dramatically increases the oxygen concentration by 12% and decreases the oxygen deficiency in CIO-T-2 to 4%.

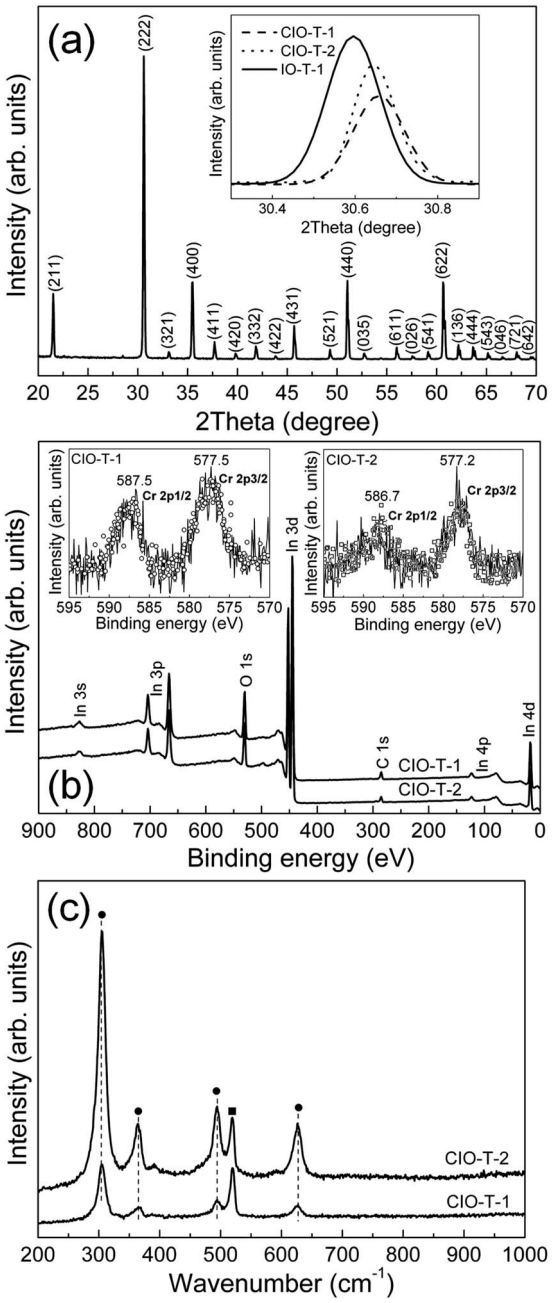

FIG. 2. (a) XRD patterns of the as-grown Cr:IO nanotower sample CIO-T-1. Inset shows the (222) peaks of the as-grown doped (CIO-T-1), the annealed doped (CIO-T-2), and the undoped (IO-T-1) samples. (b) XPS survey spectra of the samples CIO-T-1 and CIO-T-2. Insets are the detail scans of Cr $2p_{3/2}$ and $2p_{1/2}$ peaks. In the insets, solid lines and circles indicate the data taken before and after the sputtering treatment, respectively. (c) Raman spectra taken on the samples CIO-T-1 and CIO-T-2. Solid circles correspond to the IO phase (dashed line) and solid squares are due to the Si substrates.

There have been a few reports attributing RTFM to extrinsic sources such as ferromagnetic clusters or secondary phases. Raman measurements were carried out on samples

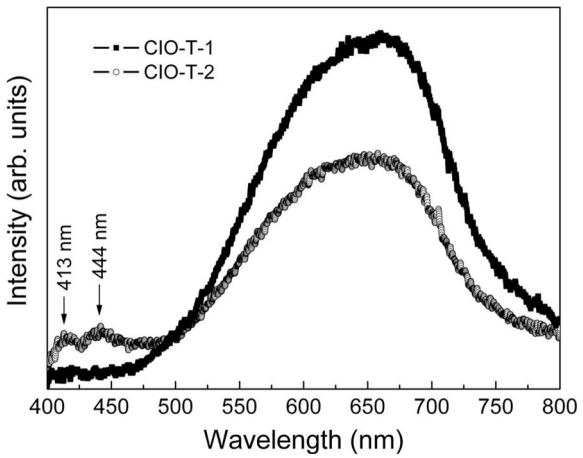

FIG. 3. PL spectra of the samples CIO-T-1 and CIO-T-2 taken at room temperature.

CIO-T-1 and CIO-T-2 and there was no Cr-related secondary phase within the detection limit, as shown in Fig. 2(c). IO has the cubic *C*-type rare-earth oxide structure and the factor group analysis predicts $4A_g$ (Raman) $+4E_g$ (Raman) $+14T_g$ (Raman) $+5A_u$ (inactive) $+5E_u$ (inactive) $+16T_u$ (infrared) modes.[34] Characteristic Raman peaks appear at 308, 368, 498.5, and 628.5 cm^{-1}; all the observed modes match well with the frequency positions reported for cubic IO.[34]

The oxygen deficiency in the IO-based samples strongly affects their optical properties. To the best of our knowledge, photoluminescence studies have not been reported before for one-dimensional transition-metal-doped IO nanomaterials. We used RT PL excited by a He-Cd laser (325 nm) to investigate the optical properties and the band structures of the nanotowers. As shown in Fig. 3, CIO-T-1 and CIO-T-2 exhibit broad orange-red emission peak at ~640 nm, which has been previously reported in undoped IO thin films and was attributed to oxygen vacancies.[35] In the photoexcitation process, the emission results from the radiative recombination of the photogenerated holes with the electrons induced by the Cr doping and the ionized oxygen vacancies. Some theoretical calculations have suggested that the large oxygen deficiency in IO should be attributed to oxygen vacancies instead of cation interstitials.[36] Compared with the annealed sample (CIO-T-2), the stronger visible emission in the as-grown sample (CIO-T-1) reflects its higher oxygen deficiency, which confirms the XPS results. Moreover, there exist another two peaks at 413 and 444 nm for CIO-T-2, which could be related to the near-band-edge emission.[37] The appearance of these two peaks indicates an improved crystal structure and fewer defects in CIO-T-2, consistent with the XRD results.

After determining the levels of oxygen deficiency in the as-grown and annealed Cr:IO samples, we carried out the magnetic measurements using a SQUID magnetometer. Figure 4(a) shows the raw magnetization versus applied magnetic-field (*M-H*) data measured at 5 and 300 K for CIO-T-1 and CIO-T-2 without subtracting the substrate contribution; it is clear that there is a ferromagnetic component in the *M-H* curves. In order to exclude the effect of any potential contamination of the substrates that may contribute to the observed ferromagnetism, we measured the silicon substrates using the same procedures. As shown in Fig. 4(b), the bare substrate exhibits only diamagnetic behavior. The diamagnetic backgrounds of the silicon substrates were subtracted from the raw data according to the sample weights. Typically the magnetic signals after substrate subtraction are on the order of 10^{-4} emu. The weights of nanotowers were determined after chemical etching and the magnetic moments were calculated. Figure 4(c) shows the *M-H* data measured at 5 and 300 K for CIO-T-1 and CIO-T-2 after subtraction of

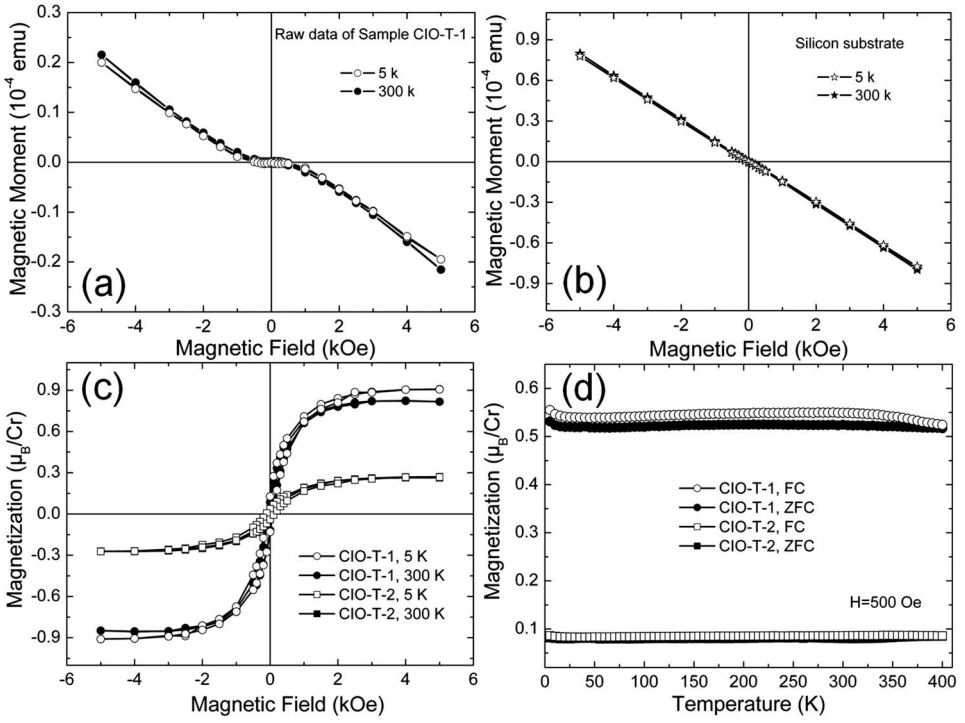

FIG. 4. (a) Raw *M-H* data without the subtraction of the substrate contribution measured on as-grown Cr:IO nanotower sample CIO-T-1 at 5 and 300 K. (b) *M-H* data taken on a silicon substrate showing the diamagnetic behavior. (c) *M-H* loops of the as-grown sample CIO-T-1 and the annealed sample CIO-T-2 taken at 5 and 300 K. (d) ZFC and FC magnetization curves of the as-grown sample CIO-T-1 and the annealed sample CIO-T-2.

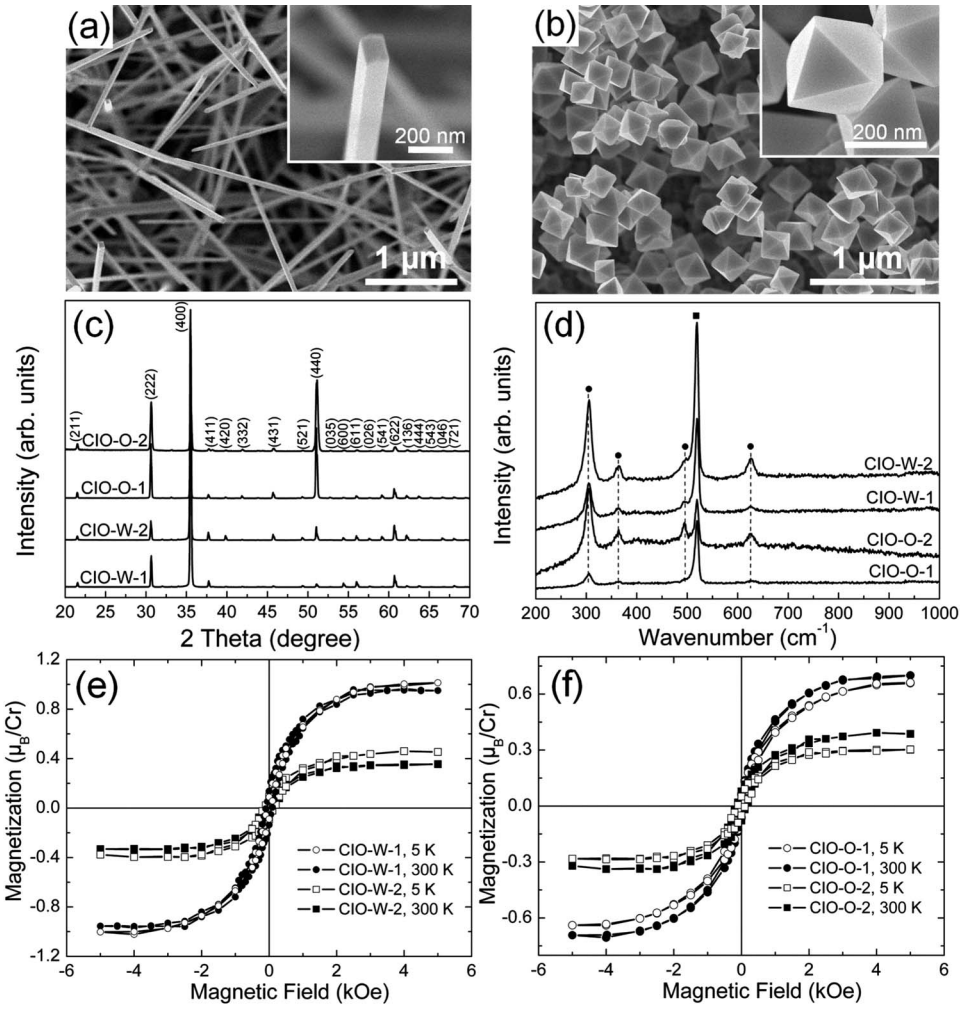

FIG. 5. FESEM images of (a) Cr:IO nanowires and (b) Cr:IO octahedrons. Insets show the corresponding high-magnification images. (c) XRD patterns of samples CIO-W-1, CIO-W-2, CIO-O-1, and CIO-O-2, respectively. (d) Raman spectra taken on the samples CIO-W-1, CIO-W-2, CIO-O-1, and CIO-O2. Solid circles correspond to the IO phase (dashed line) and solid squares are due to the Si substrates. (e) *M-H* loops of the samples CIO-W-1 and CIO-W-2 taken at 5 and 300 K. (f) *M-H* loops of samples CIO-O-1 and CIO-O-2 taken at 5 and 300 K.

the diamagnetic substrate contribution. Both Cr:IO nanotower samples exhibit clear hysteresis loops, suggesting RTFM. For the as-grown sample CIO-T-1, the coercive field and the saturation magnetization at 300 K are 59 Oe and 0.81 μ_B/Cr, respectively, which is in agreement with the previous results obtained on oxygen-deficient Cr:IO thin films.[18] With an applied field of 500 Oe, both the zero-field cooled (ZFC) and the field cooled (FC) measurements were performed and the data are shown in Fig. 4(d). However, without high-temperature measurement, T_c cannot be determined. Importantly, we found that the magnetic properties are closely correlated with the oxygen concentration: the saturated RT magnetic moment of CIO-T-1 is almost four times stronger than that of CIO-T-2.

IV. STRONG CORRELATION BETWEEN FERROMAGNETISM AND OXYGEN DEFICIENCY

In order to gain insight on the origin of the magnetism in Cr:IO, we carried out a systematic and comparative study on Cr:IO nanostructures comprising not only nanotowers but also nanowires and octahedrons. It is well known that RTFM in DMS is often linked with extrinsic origins such as unintentional sample contamination and metal clustering. Since doped IO samples with distinct morphologies were synthesized with different growth conditions, a comparative study may help to reveal the dominant parameters and to elucidate the underlying mechanism. Furthermore, these nanomaterials are characterized with different levels of oxygen deficiency, which we hypothesize may affect their magnetic properties. As we will show, indeed, oxygen deficiency dictates the strength of ferromagnetism in Cr:IO samples. Cr:IO nanowire and octahedron structures were grown on the silicon substrates by adjusting the growth temperature and the source content. As listed in Table I, the as-grown nanowire, the annealed nanowire, the as-grown octahedron, and the annealed octahedron Cr:IO samples were named as CIO-W-1, CIO-W-2, CIO-O-1, and CIO-O-2, respectively. Figures 5(a) and 5(b) are the FESEM images taken on the nanowire and the octahedron samples. The Cr:IO nanowires typically have a length of ~10 μm and a rectangular cross section with a dimension of 100–200 nm. The octahedron surfaces comprise of eight equilateral triangles with a typical side length of ~200 nm. Their morphologies and dimensions are comparable to those of undoped IO nanowires and octahedrons reported previously.[38] We found that Cr doping does not affect the morphology and the density of the growth products. The structural and compositional characteristics of the nanowire and the octahedron samples were investigated by XRD, Raman, and XPS measurements. In Fig. 5(c), the XRD results indicate that there was no detectable impurity phase in

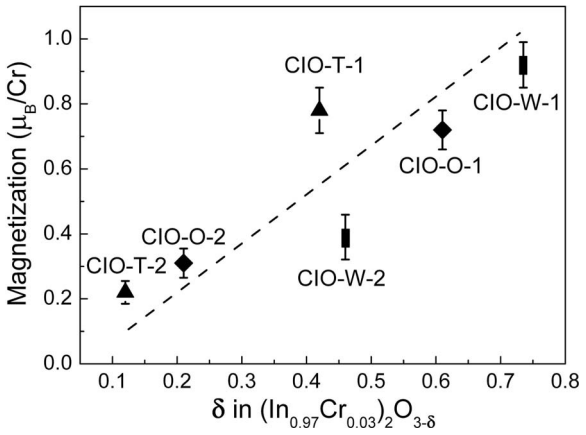

FIG. 6. Room-temperature magnetizations of the samples CIO-T-1, CIO-T-2, CIO-W-1, CIO-W-2, CIO-O-1, and CIO-O-2 versus the corresponding levels of oxygen deficiency. The dashed line is to guide the eyes.

the as-grown and the annealed samples CIO-W-1, CIO-O-1, CIO-W-2, and CIO-O-2. XPS characterizations were also performed and the nonstoichiometric formula for CIO-W-1, CIO-W-2, CIO-O-1, and CIO-O-2 are $(In_{0.97}Cr_{0.03})_2O_{2.28}$, $(In_{0.97}Cr_{0.03})_2O_{2.55}$, $(In_{0.97}Cr_{0.03})_2O_{2.40}$, and $(In_{0.97}Cr_{0.03})_2O_{2.80}$, respectively. Therefore, the Cr doping levels are the same for the nanotower, nanowire, and octahedron samples. Importantly, these samples show different levels of oxygen deficiency; air annealing always helps to increase the oxygen content. Figure 5(d) shows the Raman spectra of the samples CIO-W-1, CIO-W-2, CIO-O-1, and CIO-O-2, and no additional peak due to Cr doping was observed.

The magnetic behaviors of Cr:IO nanowires and octahedrons are similar to what observed on Cr:IO nanotowers. As shown in Figs. 5(e) and 5(f), both CIO-W-1 and CIO-O-1 show clear hysteresis loops at 5 and 300 K, which indicates RTFM. For the nanowire samples, the RT saturation magnetic moment decreases from 0.95 μ_B/Cr in the as-grown sample CIO-W-1 to 0.35 μ_B/Cr in the annealed sample CIO-W-2. A similar decrease from 0.72 μ_B/Cr to 0.31 μ_B/Cr was observed in the octahedron samples. In general, annealed samples always exhibit weakened magnetism; this trend is also consistent with the observations on Cr:IO nanotower samples.

A comparative study on the as-grown and the annealed Cr:IO nanotower, nanowire, and octahedron samples revealed a strong correlation between the ferromagnetism and the oxygen deficiency. The room-temperature saturation magnetizations of the Cr:IO nanostructures CIO-T-1, CIO-T-2, CIO-W-1, CIO-W-2, CIO-O-1, and CIO-O-2 versus their corresponding levels of oxygen deficiency are shown in Fig. 6. For this particular material system of Cr:IO, the trend is quite clear: the ferromagnetism is enhanced by the oxygen deficiency. Previous studies from other groups also suggested that the oxygen deficiency plays a critical role in the onset of ferromagnetism.[18] In these reports on Cr:IO thin films, the oxygen content was controlled by the background oxygen pressure during deposition.[18] We should note that unlike the conventional thin-film synthesis the vapor transport method often does not allow a wide-range tuning of the oxygen content in the inert carrying gas during the nanostructure growth. The supersaturation of the metal vapors and the oxygen-poor environment often result into severe oxygen deficiency in the as-grown nanostructures. Indeed, our results indicate that the particular growth method used to produce Cr:IO nanotowers, nanowires, and octahedrons consistently lead to a high degree of oxygen deficiency. For the as-grown and the annealed samples, even if the quantitative levels of the oxygen deficiency may not be accurately determined by fitting the XPS data, the qualitative comparison between the samples is still valid and the trend revealed in Fig. 6 is unambiguous.

This strong correlation between the ferromagnetism and the oxygen deficiency must be taken into account in order to understand the origin of the observed RTFM. Since the prediction and discovery of DMS, there is still a lack of unified models to explain the experimental observations on a wide range of materials from a variety of synthesis methods. The discrepancies frequently appear due to extrinsic factors such as intentional contaminations and clustering of doping elements which could contribute to weak magnetism. In the present study, we took extra care to avoid any source of contamination by means such as using plastic tweezers and checking straws used in the SQUID measurements. We also believe that the clustering of Cr or the formation of CrO_2 cannot account for the observed magnetism. Although the ferromagnetic CrO_2 has a T_c of 396 K, its pure phase is difficult to synthesize.[39] Besides, the XPS data in Fig. 2(b) suggests that most Cr ions have the +3 valence and likely replace the In ions in the IO matrix.

The low Cr doping concentration does not favor the conventional short-range superexchange or double exchange mechanism as the origin of the observed RTFM. In such a low-spin-concentration regime, the long-range ferromagnetic ordering may be established if the carrier-mediated exchange interaction is effectively ferromagnetic as suggested in the Ruderman-Kittel-Kasuya-Yosida and the Zener models.[4] On the other hand, the strong correlation between the ferromagnetism and the oxygen deficiency suggests that the formation of bound magnetic polarons may dictate the magnetic ordering in our samples. Donor electrons from the oxygen vacancies mediate the ferromagnetic coupling between impurities within the hydrogenic orbits.[40,41] The radius of the hydrogenic orbits is given by $r_H=\varepsilon(m/m^*)a_0$, where ε is the high-frequency dielectric constant, m is the electron mass, m^* is the effective mass of the donor electrons, and a_0 is the Bohr radius (53 p.m.).[41] For IO, $\varepsilon=9$ and $m^*/m=0.3$ give r_H of 1.6 nm, which is much larger than the values for ZnO (0.76 nm), TiO_2 (0.48 nm), and SnO_2 (0.86 nm). Therefore, in IO, a lower level of oxygen deficiency may be required to create a spin-split impurity band and to trigger the percolative transition from para- to ferromagnetic ordering. A general characteristic of the bound magnetic polarons model is that a high level of oxygen vacancies is a prerequisite to reach the percolation threshold for the onset of ferromagnetic ordering, which is readily satisfied in the as-grown oxygen-deficient Cr:IO samples.

We also found that the oxygen vacancies alone are not adequate to establish a robust ferromagnetism; the Cr doping

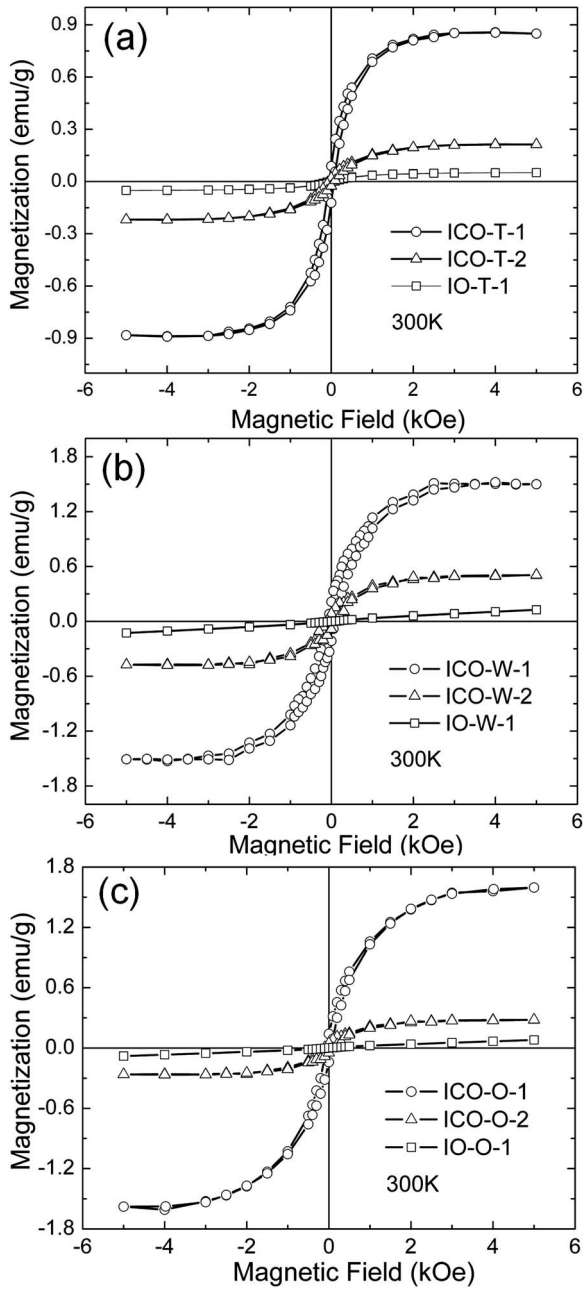

FIG. 7. Comparison of *M-H* loops taken at 300 K on (a) nanotower samples CIO-O-1, CIO-O-2, and IO-T-1; (b) nanowire samples CIO-W-1, CIO-W-2, and IO-W-1; (c) octahedron samples CIO-O-1, CIO-O-2, and IO-O-1.

is dispensable. Figure 7 compared the *M-H* loops of the as-grown and the annealed Cr-doped samples with those of the undoped counterparts. The as-grown undoped nanotower, nanowire, and octahedron samples are also oxygen deficient; from the XPS results their nonstoichiometric formula can be written as $In_2O_{2.57}$, $In_2O_{2.29}$, and $In_2O_{2.42}$ for IO-T-1, IO-W-1, and IO-O-1, respectively. Although the oxygen-deficient undoped IO samples also show modest ferromagnetic behaviors at RT, their magnetism is more than ten times weaker than that of the as-grown Cr:IO samples. This observation is consistent with the report by Hong *et al.*,[42] who observed that the magnetic moments in IO films are much smaller than those in TiO_2 and HfO_2 films. Thus both the Cr doping and the oxygen vacancies are critical to establish stable RTFM in IO-based DMS. The interplay between the Cr ions and the oxygen vacancies and the possible formation of defect complex warrant further investigations.

In Cr:IO samples, the charge transfer between the host and the doped ions and the alteration of the electronic structure induced by the Cr doping and the oxygen vacancies appear to play important roles in establishing the ferromagnetism. A recent density-functional calculation showed that in Cr:IO the ferromagnetic Cr-Cr interaction can be tuned and even switched via electron doping.[22] Although Cr itself may not produce any free electrons,[22] the extrinsic additional electrons doping, such as the large amount of donors induced by oxygen vacancies could provide the needed carriers to stabilize the long-range ferromagnetic ordering.[22] Since the partially filled Cr 3*d* states have to interact with the impurity band to create spin-split levels, both the Cr substitutions and the oxygen vacancies must be present to stabilize the ferromagnetic ordering, which is in line with our experimental observations. On the other hand, we should note that even though IO is a prototypical *n*-type transparent conducting oxide, open questions still remain regarding to the band structures of the undoped and doped IO. A recent x-ray spectroscopic study suggested that the fundamental band gap in IO is much smaller than the widely quoted value of 3.75 eV and a Burstein-Moss shift should also be taken into account after doping.[43] Furthermore, in contrast to other semiconductors, a strong electron accumulation may occur at the IO surface,[44] which may further make the magnetic ordering surface sensitive.

Recently, spinodal decomposition and self-assembled formation of Cr-rich and Cr-poor metallic nanocrystals were observed in (Zn,Cr)Te and was suggested to account for the ferromagnetic ordering.[45] The charge state of the Cr ions and the Fermi energy can be tuned by doping and lead to a variation in the apparent T_c. In our experiments, the HRTEM (JEM-2100F) equipped with energy dispersive spectroscopy (EDS) has an analytical probe size of 0.5 nm. The spatial resolution in the mapping plane was about 5 nm, comparable to that reported in Ref. 45. Both the HRTEM imaging and the EDS mapping did not reveal any nonuniform Cr distribution or the formation of Cr-rich nanocrystals. Furthermore, as we shown in Fig. 2(b), the Cr peak position in the XPS spectra suggests that the majority of the doped Cr ions are Cr^{3+}, which may replace the In ions in the IO matrix. However, the attractive force between the metal ions may still drive the spinodal decomposition to a certain degree, which should be evaluated and warrant further studies.

V. CONCLUSIONS

In summary, a comprehensive study on the RTFM has been carried out on the Cr:IO nanotowers, nanowires, and octahedrons grown with a vapor transport technique. XRD, HRTEM, Raman, and XPS measurement results confirmed the Cr doping and indicated no secondary phase or cluster

formation within the detection limits. In this study, we focused on isolating the effect of oxygen vacancies and found a strong correlation between the enhanced ferromagnetism in the as-grown samples with the high-oxygen deficiency levels. This correlation suggests a defect-mediated mechanism; both the oxygen vacancies and the Cr dopants play critical and complimentary roles to alter the electronic band structure of the IO host and to stabilize the long-range ferromagnetic ordering. Further experiments of magnetotransport on individual nanostructures and x-ray magnetic circular dichroism studies are currently under way to investigate the mechanism in more details and to explore the possibility of constructing nanoscale transparent spintronic devices.

ACKNOWLEDGMENTS

This research was supported by Nanyang Technological University Research Grant No. SUG 20/06 RG and Institute of Materials Research and Engineering.

*Corresponding author; tomwu@ntu.edu.sg

[1] H. Ohno, Science **281**, 951 (1998).
[2] S. A. Wolf, D. D. Awschalom, R. A. Buhrman, J. M. Daughton, S. von Molnar, M. L. Roukes, A. Y. Chtchelkanova, and D. M. Treger, Science **294**, 1488 (2001).
[3] S. J. Pearton, C. R. Abernathy, M. E. Overberg, G. T. Thaler, D. P. Norton, N. Theodoropoulou, A. F. Hebard, Y. D. Park, F. Ren, J. Kim, and L. A. Boatner, J. Appl. Phys. **93**, 1 (2003).
[4] T. Dietl, H. Ohno, F. Matsukura, J. Cibert, and D. Ferrand, Science **287**, 1019 (2000).
[5] Y. Matsumoto, M. Murakami, T. Shono, T. Hasegawa, T. Fukumura, M. Kawasaki, P. Ahmet, T. Chikyow, S.-y. Koshihara, and H. Koinuma, Science **291**, 854 (2001).
[6] S. B. Ogale, R. J. Choudhary, J. P. Buban, S. E. Lofland, S. R. Shinde, S. N. Kale, V. N. Kulkarni, J. Higgins, C. Lanci, J. R. Simpson, N. D. Browning, S. Das Sarma, H. D. Drew, R. L. Greene, and T. Venkatesan, Phys. Rev. Lett. **91**, 077205 (2003).
[7] J. M. Baik and J.-L. Lee, Adv. Mater. **17**, 2745 (2005).
[8] O. D. Jayakumar, I. K. Gopalakrishnan, and S. K. Kulshreshtha, Adv. Mater. **18**, 1857 (2006).
[9] G. Z. Xing, J. B. Yi, J. G. Tao, T. Liu, L. M. Wong, Z. Zhang, G. P. Li, S. J. Wang, J. Ding, T. C. Sum, C. H. A. Huan, and T. Wu, Adv. Mater. **20**, 3521 (2008).
[10] C. Klingshirn, ChemPhysChem **8**, 782 (2007).
[11] I. Hamberg and C. G. Granqvist, J. Appl. Phys. **60**, R123 (1986).
[12] C. G. Granqvist and A. Hultlker, Thin Solid Films **411**, 1 (2002).
[13] N. H. Hong, J. Sakai, N. T. Huong, and V. Brizé, Appl. Phys. Lett. **87**, 102505 (2005).
[14] N. H. Hong, J. Sakai, N. T. Huong, A. Ruyter, and V. Brizé, J. Phys.: Condens. Matter **18**, 6897 (2006).
[15] G. Peleckis, X. L. Wang, and S. X. Dou, Appl. Phys. Lett. **88**, 132507 (2006).
[16] S. J. Hu, S. S. Yan, X. L. Lin, X. X. Yao, Y. X. Chen, G. L. Liu, and L. M. Mei, Appl. Phys. Lett. **91**, 262514 (2007).
[17] D. W. Chu, Y. P. Zeng, and D. L. Jiang, Appl. Phys. Lett. **92**, 182507 (2008).
[18] J. Philip, A. Punnoose, B. I. Kim, K. M. Reddy, S. Layne, J. O. Holmes, B. Satpati, P. R. Leclair, T. S. Santos, and J. S. Moodera, Nature Mater. **5**, 298 (2006).
[19] P. Kharel, C. Sudakar, M. B. Sahana, G. Lawes, R. Suryanarayanan, R. Naik, and V. M. Naik, J. Appl. Phys. **101**, 09H117 (2007).
[20] L. Bizo, M. Allix, H. Niu, and M. J. Rosseinsky, Adv. Funct. Mater. **18**, 777 (2008).
[21] P. F. Xing, Y. X. Chen, Y. Shi-Shen, G. L. Liu, L. M. Mei, K. Wang, X. D. Han, and Z. Zhang, Appl. Phys. Lett. **92**, 022513 (2008).
[22] H. Raebiger, S. Lany, and A. Zunger, Phys. Rev. Lett. **101**, 027203 (2008).
[23] D. W. Chu, Y. P. Zeng, D. L. Jiang, and Z. M. Ren, Appl. Phys. Lett. **91**, 262503 (2007).
[24] M. A. Garcia, J. M. Merino, P. E. Fernandez, A. Quesada, J. de la Venta, G. M. L. Ruiz, G. R. Castro, P. Crespo, J. Llopis, and J. M. Gonzalez-Calbet, Nano Lett. **7**, 1489 (2007).
[25] Z. Zhang, S. J. Wang, T. Yu, and T. Wu, J. Phys. Chem. C **111**, 17500 (2007).
[26] Z. Zhang, Y. H. Sun, Y. G. Zhao, G. P. Li, and T. Wu, Appl. Phys. Lett. **92**, 103113 (2008).
[27] R. S. Wagner and W. C. Ellis, Appl. Phys. Lett. **4**, 89 (1964).
[28] H. J. Fan, R. Scholz, M. Zacharias, U. Gösele, F. Bertram, D. Forster, and J. Christen, Appl. Phys. Lett. **86**, 023113 (2005).
[29] J. B. Hannon, S. Kodambaka, F. M. Ross, and R. M. Tromp, Nature (London) **440**, 69 (2006).
[30] Y. G. Yan, Y. Zhang, H. B. Zeng, and L. D. Zhang, Cryst. Growth Des. **7**, 940 (2007).
[31] R. D. Shannon and C. T. Prewitt, Acta Crystallogr. B **25**, 925 (1969).
[32] C. Xu, M. Hassel, H. Kuhlenbeck, and H. J. Freund, Surf. Sci. **258**, 23 (1991).
[33] N. J. C. Ingle, R. H. Hammond, and M. R. Beasley, J. Appl. Phys. **89**, 4631 (2001).
[34] W. B. White and V. G. Keramidas, Spectrochim. Acta, Part A **28**, 501 (1972).
[35] M.-S. Lee, W. C. Choi, E. K. Kim, C. K. Kim, and S.-K. Min, Thin Solid Films **279**, 1 (1996).
[36] S. Lany and A. Zunger, Phys. Rev. Lett. **98**, 045501 (2007).
[37] H. Q. Cao, X. Q. Qiu, Y. Liang, Q. M. Zhu, and M. J. Zhao, Appl. Phys. Lett. **83**, 761 (2003).
[38] Y. F. Hao, G. W. Meng, C. H. Ye, and L. D. Zhang, Cryst. Growth Des. **5**, 1617 (2005).
[39] L. Ranno, A. Barry, and J. M. D. Coey, J. Appl. Phys. **81**, 5774 (1997).
[40] A. Kaminski and S. Das Sarma, Phys. Rev. Lett. **88**, 247202 (2002).
[41] J. M. D. Coey, M. Venkatesan, and C. B. Fitzgerald, Nature Mater. **4**, 173 (2005).
[42] N. H. Hong, J. Sakai, N. Poirot, and V. Brizé, Phys. Rev. B **73**, 132404 (2006).
[43] A. Walsh, J. L. F. Da Silva, S. H. Wei, C. Korber, A. Klein, L. F.

J. Piper, A. DeMasi, K. E. Smith, G. Panaccione, P. Torelli, D. J. Payne, A. Bourlange, and R. G. Egdell, Phys. Rev. Lett. **100**, 167402 (2008).

[44] P. D. C. King, T. D. Veal, D. J. Payne, A. Bourlange, R. G. Egdell, and C. F. McConville, Phys. Rev. Lett. **101**, 116808 (2008).

[45] S. Kuroda, N. Nishizawa, K. Takita, M. Mitome, Y. Bando, K. Osuch, and T. Dietl, Nature Mater. **6**, 440 (2007).